Comparison of Supercritical Airfoil Flow Calculations with Wind Tunnel Results

L. S. King* and D. A. Johnson†
NASA Ames Research Center, Moffett Field, California

Navier-Stokes calculations are performed for a supercritical airfoil at transonic design and subsonic conditions. Wind tunnel pressure-rail measurements are employed as boundary data in the calculations to account for wall-interference effects. A fine mesh is used so that most details of the flows were resolved, with particular attention given to the trailing-edge region. Detailed comparisons are made with the experimental data. Good agreement was obtained on the airfoil except at the trailing edge where separation occurred. Flow details in the trailing-edge region are examined and differences are shown to be attributable to the turbulence model employed.

Introduction

SUPERCRITICAL airfoils are characterized by a nearly flat upper surface over a large midchord distance and a pronounced camber near the trailing edge. These characteristics combine to make the performance of these airfoils very sensitive to wind tunnel wall interference effects, viscous effects, and small changes in Mach number and angle of attack. Because of the relatively flat upper surface, shock position is quite sensitive to wall interference. Because of the aft camber, there exists a strong adverse pressure gradient near the trailing edge. This leads to a thickening and, often, to a separation of the upper-surface boundary layer. Also, because of the aft camber, significant static-pressure differences exist across the near wake. Interferometric measurements by Spaid and Bachalo[1] and the laser-velocimeter results of Johnson and Spaid[2] have verified the existence of these pressure differences. The pressure difference across the wake is, of course, related to wake curvature, and it has been suggested that curvature effects are important in the prediction of surface-pressure distributions.[3,4]

A supercritical airfoil section thus presents a predictive method with many difficulties. To date, predictions have not compared well with wind tunnel data, as evidenced by the results presented in Ref. 5. Since the numerical solutions were for free-air flows, wall-interference effects in the data could be a factor in the poor comparison. Other possible contributors are improper turbulence closure models and inadequate spatial resolution. Thus, questions arise as to the validity of such comparisons.

The present effort will attempt to resolve some of these questions. Navier-Stokes calculations are performed on a fine mesh. Wind tunnel wall effects are simulated by using measured pressures as boundary data along the upper and lower computational boundaries. Johnson and Spaid[2] have obtained extensive measurements for the DSMA 671 supercritical section. Turbulence properties and mean velocities were measured in the boundary layer and wake. These data thus offer an excellent opportunity for detailed comparison with calculated results. Because a fine mesh is used and the wall effects are accounted for, any substantial differences between experimental results and calculations should be attributable primarily to inadequacies in the turbulence model. Since experimental data are imposed on the outer computational boundary, such an approach falls short of being an independent predictive tool. Nevertheless, the method is useful in that: 1) direct comparisons between numerical and experimental results may be made; 2) by also performing free-air calculations, differences between interference-free and confined flows may be illustrated; and 3) turbulence researchers are provided with a tool to enable valid comparisons of measured and modeled turbulence properties on an airfoil.

Other methods have been developed to eliminate or reduce wall-interference effects in transonic flow. Of particular interest here are the correction methods developed by Kemp[6-8] and Murman.[9] In these methods, flowfield and surface-pressure measurements are employed to calculate either an effective airfoil shape or velocity jumps between the upper and lower surfaces. These are then used in free-air inviscid calculations to determine the angle of attack and Mach number that best fit the surface measurements. Through use of the measured pressures, these methods accommodate wall effects without recourse to modeling the wall-flow processes. They also account, at least partially, for viscous effects. However, interference and viscous effects may render the measured pressures on the airfoil incompatible with any inviscid free-air solution, in which case correction methods are not applicable. If corrected values of Mach number and angle of attack can be found, an equivalent free-air solution can be computed using the Navier-Stokes code. Comparison of this solution with experiment and the pressure-boundary-condition solution provides insight into the correctability of these supercritical airfoil flows.

Numerical Procedure

The basic numerical method used in the present investigation is that due to Steger[10] for the Reynolds-averaged, time-dependent, compressible Navier-Stokes equations. In Steger's method, the governing equations are transformed into a generalized body-fitted coordinate system and solved with the second-order-accurate factorized implicit algorithm of Beam and Warming.[11,12] Viscous terms in the streamwise direction are neglected, resulting in the so-called "thin-layer approximation." Turbulence is modeled by the Baldwin-Lomax[13] adaptation of the algebraic turbulence model of Cebeci.[14] To account for wind tunnel wall interference effects, Steger's code has been modified by incorporating a pressure boundary condition (PBC) along the upper and

Presented as Paper 83-1688 at the AIAA 16th Fluid and Plasma Dynamics Conference, Danvers, Mass., July 13-15, 1983; received Oct. 22, 1983; revision received Oct. 8, 1984. This paper is declared a work of the U.S. Government and therefore is in the public domain.

*Research Scientist.
†Research Scientist. Member AIAA.

lower boundaries. Details of this modification are presented in an earlier paper by King and Johnson.[15]

Mesh generation is accomplished using a Poisson solver similar to that of Thompson et al.,[16] as modified by Steger and Sorenson.[17] The mesh code produces a "wraparound" or C-mesh and is coincident with user-prescribed points on the airfoil surface and outer boundary. With the Steger-Sorenson modification, orthogonality at the airfoil surface and concentration of coordinate lines near the surface may be controlled. Orthogonality is needed for consistency with the thin-layer approximation. A fine mesh near the surface is required to resolve the turbulent boundary layer properly. Typically, meshes used in the present calculations were comprised of 139 points in the wraparound direction and 50 points in the direction away from the airfoil. The meshes were constructed with the first coordinate line off the airfoil at a normal distance of 2×10^{-5} chords from the surface. This distance roughly corresponds to a value of $y^+=2$, with approximately 20 points in the turbulent boundary layer near the airfoil midchord.

Results and Discussion

The airfoil employed in the present investigation is the 14%-thick supercritical section known as DSMA 671. This airfoil was tested in the Ames 2×2 ft Transonic Wind Tunnel by Johnson and Spaid.[2] Subsequent to that test, additional testing was done to obtain the pressure rail measurements and to take holographic interferograms. The model for the tests had a chord of 20.32 cm (8 in.) and an aspect ratio of 3. These Ames tests were conducted at a chord Reynolds number of 2.67 million with transition strips at 17% chord to ensure fully turbulent boundary layers. Data were obtained at two test conditions: a cruise condition of $M=0.72$ and an angle of attack of 4.32, and a subcritical case at $M=0.50$ and an angle of attack of 5.35. In addition to surface pressures, boundary-layer and near-wake measurements were made with pitot-pressure-probe and laser-velocimeter techniques. The holographic interferograms taken of the flowfields are described by Bachalo.[18]

The pressure rails were a special feature incorporated so that the PBC calculations could be performed. The rails were designed to measure the static-pressure distribution along the tunnel centerline and 7.62 cm (3 in.) from the upper and lower tunnel walls. Since the model chord was 20.32 cm (8 in.) the rail pressure measurements were made at $y/c=\pm1.125$. Shown in Fig. 1 are the rail pressure distributions: Fig. 1a shows the pressures at the subcritical case ($M=0.5$, $\alpha=5.35$ deg), and Fig. 1b shows that for the transonic cruise condition ($M=0.72$, $\alpha=4.32$ deg). As can be seen, there was scatter in the pressure rail measurements. This was due in part to difficulties encountered with the Scanivalve system during the test. Also, the rail pressures differ from the freestream pressure by only 5% maximum. Consequently, there are uncertainties as to the pressures to be used in the PBC calculations. The fairings shown in Fig. 1 represent only a best guess for the rail pressures.

Also shown in Fig. 1 are pressures along $y/c=\pm1.125$ resulting from the free-air solution. Along the lower rail position little difference between the measured pressures and the free-air pressures is noted. Incidentally, the free-air pressures were imposed on the lower boundary for the subcritical case. It was felt that this pressure distribution was a good approximation because of the scatter in the data. Along the upper rail position, however, much larger differences exist between the free-air and measured pressures.

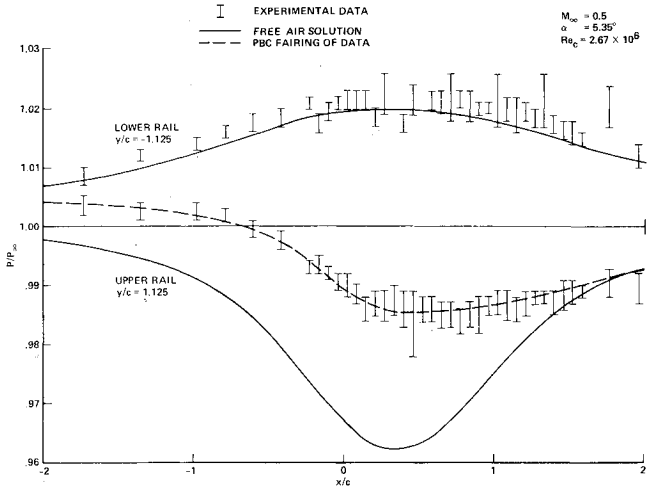

a) Subcritical flow case.

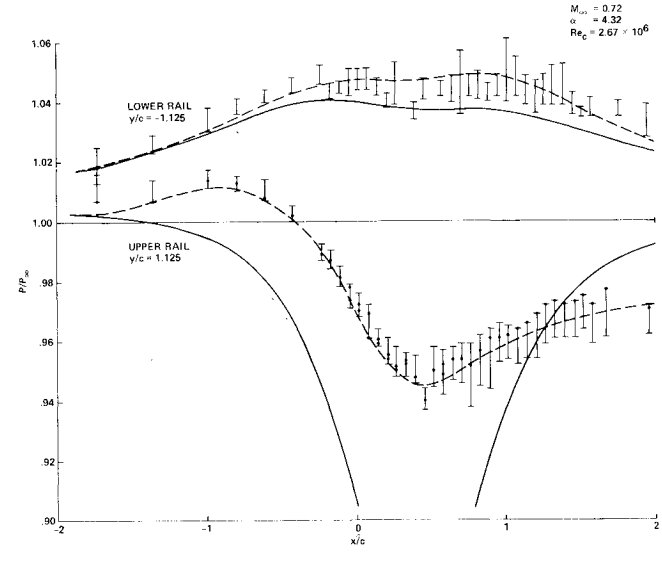

b) Transonic cruise condition.

Fig. 1 Pressure distributions in the flowfield at the pressure rail locations.

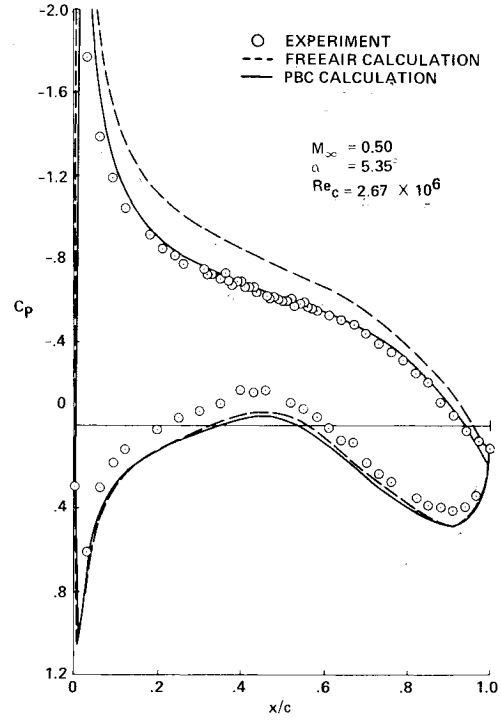

Fig. 2 Surface pressures for subcritical flow case.

Surface-Pressure Comparisons

The fact that the upper-rail pressures can create a significant difference at the airfoil surface is illustrated in Figs. 2 and 3. For the subcritical case of Fig. 2, the upper-surface pressures are brought into excellent agreement with the measured values. Separation was experimentally observed over the last 2% chord of the airfoil. Predicted separation was over the last 3% chord, but with a thinner reverse-flow region and an attendantly slightly greater pressure recovery.

For the cruise condition shown in Fig. 3, the differences between the free-air and PBC calculations are even more pronounced. Shock position varies markedly between free air and PBC, with the PBC-predicted shock in close agreement to that measured. The PBC calculation shows a slight re-expansion just downstream of the shock followed by pressure recovery to the trailing edge. Although the data indicate the same trend, the calculated re-expansion is slightly larger and the pressures remain slightly overexpanded relative to the data to near the trailing edge. This indicates, perhaps, that the fairing used for the upper-rail pressures could be improved upon. As was the case for the subcritical flow, pressure recovery at the trailing edge was slightly overpredicted. The trailing-edge region for the cruise condition is discussed in more detail in subsequent sections.

Also shown in Fig. 3 is another free-air solution run at slightly different values of Mach number and angle of attack. These values were obtained from the TWINTAN code by Kemp[8] and purport to be the corrected free-air values for which the experimental data are applicable. The measured surface and rail pressures along with the lift coefficient were input into the TWINTAN code to predict a corrected free-air value at Mach 0.696 and a corrected angle of attack of 3.38 deg. Predicted surface pressures from the Navier-Stokes code are shown rescaled to the reference Mach number of 0.72, so that Fig. 3 represents a consistent comparison of the results. On the upper surface, agreement of the corrected free-air solution to the data and PBC calculation is quite good, except that the shock is approximately 5% chord downstream of the PBC result.

On the airfoil lower surface the corrected free-air solution appears to agree better with the data than either the (uncorrected) free-air or PBC solution. The reason for this is unclear. As a matter of fact, a similar comparison for a more conventional NACA 64A010 airfoil, shown in Fig. 4, exhibits opposite results on the lower surface. A possible explanation could lie in the treatment of upstream boundary conditions. No data are available there, therefore, the upstream boundary condition was constructed from the free-air Navier-Stokes and TSFOIL[19] inviscid solutions. From these solutions the upstream boundary estimate was taken to be that solution most consistent with the measured pressures on the upper and lower rails.

Comparisons with Boundary-Layer Calculations

Boundary-layer solutions were obtained for the transonic cruise condition in Ref. 2 using the inverse boundary-layer program described in Ref. 20. This program can be run in either of two modes: direct with the pressure specified, or inverse with the wall shear specified. The boundary-layer calculations were performed in the direct mode for the airfoil upper surface using the measured surface pressures to separation. Calculations beyond separation were performed in the inverse mode.

Results from the boundary-layer calculations are compared with the PBC solution and experiment in Figs. 5 and 6. In Fig. 5 the skin friction C_f (normalized by the freestream dynamic pressure) and displacement thickness δ^*/c are shown from just downstream of the shock to the trailing edge. Experimental skin frictions were obtained by law-of-the-wall fits to the pitot probe data. Oil-flow measurements, discussed in Ref. 2, indicate that separation occurred at $x/c=0.98$, whereas the skin frictions obtained from the pitot probe data indicate attached flow at that station. Near the trailing edge, therefore, these data must be viewed guardedly.

The skin-friction results reflect the re-expansion region behind the shock (C_f increasing) and the subsequent recompression. The boundary-layer and Navier-Stokes codes predict slightly different skin frictions in the re-expansion region because the pressures are different. In the adverse-pressure-gradient region the codes agree well with each other and are in substantial agreement with the data, at least up to separation. The predicted separation point is at 95% chord, whereas the data indicate separation to be delayed farther downstream.

Displacement thicknesses from the PBC solution are consistently higher than their boundary-layer counterparts and are in reasonable agreement with the data, as shown in Fig. 5b. The Navier-Stokes code calculated the rapid rise in displacement thickness near separation better than the boundary-layer code—a fortuitous result as will be seen in a

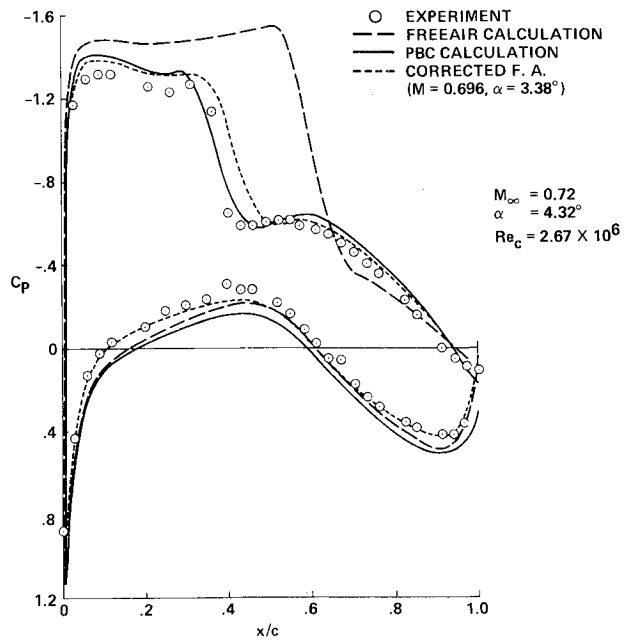

Fig. 3 Surface pressures for transonic cruise condition.

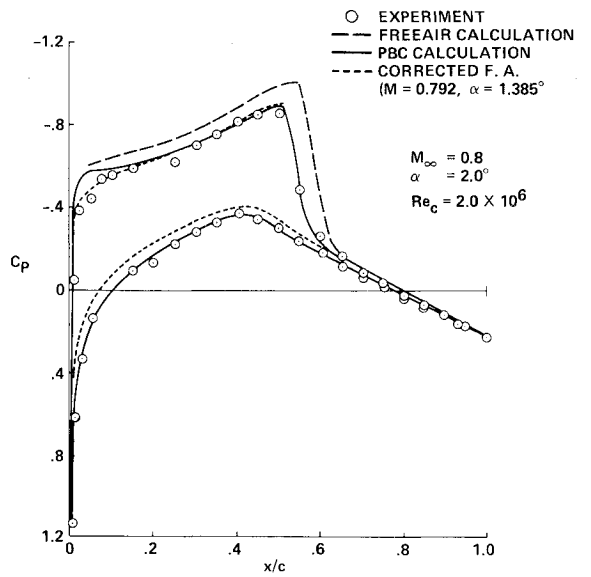

Fig. 4 Surface pressures for the NACA 64A010 airfoil.

later section. The Navier-Stokes code predicted higher displacement thicknesses near the trailing edge since the predicted pressure gradients were higher than the experimental values used in the boundary-layer code. If the PBC pressure gradient had been used in the boundary-layer code, agreement would have been much better.

Semilog plots are shown in Fig. 6 comparing the predicted and experimental velocity distributions in the boundary layer at two stations in the adverse-pressure-gradient region. The three regions of the boundary layer—the wall-damped, the law-of-the-wall, and the law-of-the-wake—can be clearly seen, indicating that the Navier-Stokes solution does have adequate resolution for the boundary layer. The boundary-layer and PBC solutions agree well with each other from the wall through the law-of-the-wall region, but depart in the law-of-the-wake region. In this latter region the boundary-layer solution agrees with the data much better than the PBC solution. This difference is almost certainly attributable to the different turbulence models employed. In the boundary-layer calculation the Cebeci-Smith model was used; the Baldwin-Lomax model was used in the Navier-Stokes calculations. The two models differ predominantly in the law-of-the-wake region, where the Steger Navier-Stokes code does not have a displacement thickness available to scale the outer eddy viscosity. Instead, Baldwin and Lomax use a distance determined from the vorticity and an additional constant that was determined to yield agreement with Cebeci and Smith for constant-pressure boundary layers at transonic speeds. It would appear that, for flows with significant pressure gradients, the Baldwin-Lomax model needs further refinement.

Trailing-Edge Flow

As has been pointed out by Horstman[21] and others,[3,4] accurate predictions in the trailing-edge region are important in airfoil design, particularly for modern supercritical sections. In this region, large streamwise adverse pressure gradients exist, and often lead to separated flow. Because of the aft camber, normal pressure gradients may become significant. In the near wake, two dissimilar shear layers interact, and pressure differences across the wake and wake curvature can become important.

The trailing-edge flow at the transonic cruise condition is presented in some detail in Figs. 7-9. In these figures the PBC solution is compared with surface-pressure data, pressures at the edge of the viscous layers deduced from laser-velocimeter measurements (using isentropic flow relations), and flow angles also derived from the laser-velocimeter measurements.

In Fig. 7, surface pressures near the trailing edge are shown together with the static pressures at the edges of the boundary layer and near wake. Across the upper-surface boundary layer, the data indicate that the pressure difference is small. The calculations show a small difference, which becomes progressively larger past the predicted separation point at $x/c = 0.95$. Although not shown, analysis of the interferometric results of Bachalo[18] indicates little pressure difference across the lower-surface boundary layer. The calculations, however, do indicate a pressure difference. This is probably a consequence of overpredicting the boundary-layer thickness, so that the calculated edge pressures are in the high-gradient inviscid flow. As seen in the figure, a large pressure difference exists across the wake at the trailing edge. This is indicative of a highly curved near wake. The data indicate that the measurable pressure difference diminishes to zero approximately 10-15% chord downstream of the trailing edge. On the other hand, the calculations show a pressure difference that decays at a slower rate.

Flow angles in the vicinity of the trailing edge are also of interest; see Figs. 8 and 9. In Fig. 8, the flow angles along the edge of the upper boundary layer and wake were predicted remarkably well by the PBC solution. The maximum

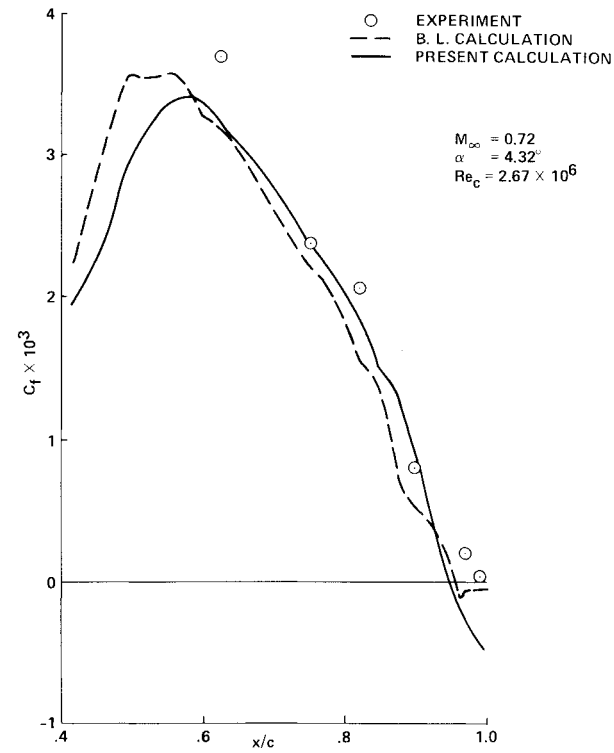

a) Skin friction.

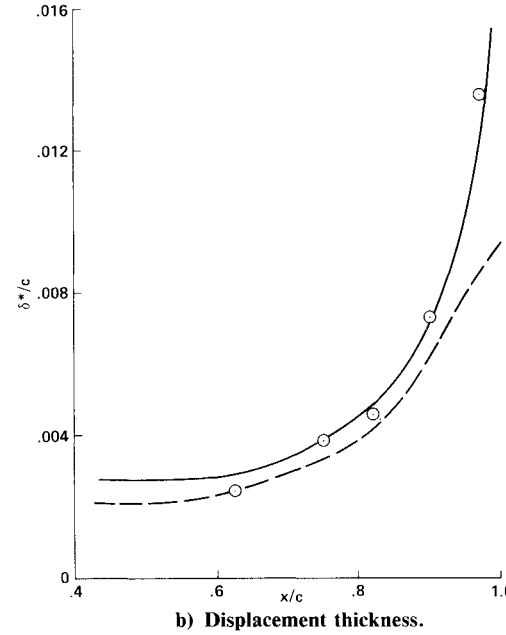

b) Displacement thickness.

Fig. 5 Skin friction and displacement thickness on the airfoil upper surface at the cruise condition.

flow angle was −14 deg at 95% chord, which is where separation is also predicted. Beyond separation, the flow angles rapidly diminish as the wake becomes horizontal. Agreement along the lower edge of the wake was not as impressive, although the correct trend is shown. The lower edge has flow angles less negative than those on the upper edge, indicative of a converging flow and necessary to maintain a pressure difference across the wake.

The laser-velocimeter data of Ref. 2 showed a jump in the flow angles near $y = 0$ in the near wake at $x/c = 1.02$ (Fig. 9). At that wake station, the flow angles vary from −12 deg at the upper edge to −24 deg just above the trailing edge. Then the flow angle jumps to about 0 deg, and almost immediately

flattens out to approximately −4.5 deg at the lower edge. The predicted flow-angle variation at this wake station was not too extreme. The flow angle at the upper edge was in good agreement with the data, but the maximum flow deflection just above $y=0$ was missed completely, as was the jump. Below $y=0$, the predicted flow angles vary smoothly from a value of −14.5 deg to the edge value of approximately −7 deg, a significantly different distribution than that observed experimentally. Further insight into these discrepancies may be obtained through examination of the velocity profiles.

Velocity and Turbulent Shear-Stress Distributions

Shown in Figs. 10-12 are the velocity and turbulent shear-stress distributions in the upper boundary layer and wake for the transonic cruise condition. It should be noted that the data and predictions included in all of these figures lie along lines normal to the wind tunnel centerline. The usual practice for presenting boundary-layer profiles is to align the coordinate system so that distances and velocities are tangent and normal to the airfoil surface. Thus, some care should be taken in interpreting the present results. The velocity profiles shown in Figs. 10 and 12 are of the horizontal velocity ratio, u/u_∞. Computed turbulent shear stress, shown in Fig. 11, is based on the normal gradient of the tangential velocity and eddy viscosity. This causes some difficulties since the experimental turbulent shear stress $-\overline{U'V'}/U_\infty^2$ was determined by correlating the horizontal and vertical fluctuating velocity components in Ref. 2. Johnson and Spaid estimate that the vertical fluctuating velocity would be reduced by about 20% if rotated to a surface-aligned coordinate system at $x/c=0.63$. Accordingly, the measured turbulent shear stresses will appear higher than they actually are, particularly toward the trailing edge.

Upper-surface boundary-layer velocity profiles are shown in Fig. 10 at four chordwise stations downstream of the shock. The first two calculated profiles, at x/c values of 0.63 and 0.75, apparently show reasonably good agreement with the data. However, semilog plots of the profiles (Fig. 6) demonstrated that the wake region of each profile had reduced gradients resulting in a larger boundary-layer thickness. At the 0.90 and 0.99 stations the prediction compares less favorably with the data. Not only are problems evident in the wake region of the profiles, but the gradients in the near-wall region are predicted to be too high. The predicted profile at $x/c=0.99$ shows the occurrence of separation. Separation has also occurred experimentally, although the laser-velocimeter data in Fig. 10 does not extend close enough to the surface to show reversed flow. The experimental profile shows low velocity gradients near the wall, whereas the

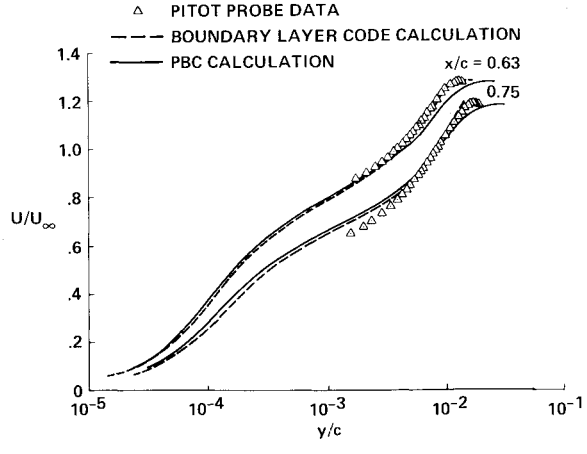

Fig. 6 Comparison of calculated results with boundary-layer theory and experimental results for velocity distributions in the upper-surface boundary layer.

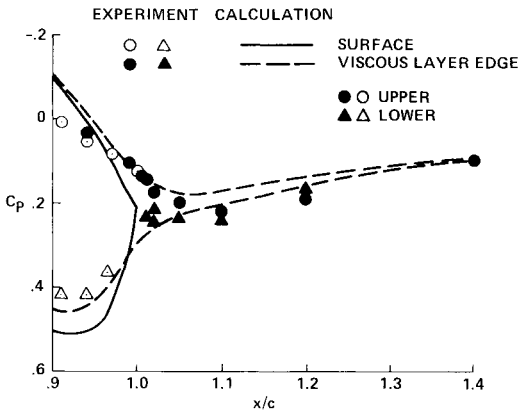

Fig. 7 Trailing-edge and near-wake static pressures at cruise condition.

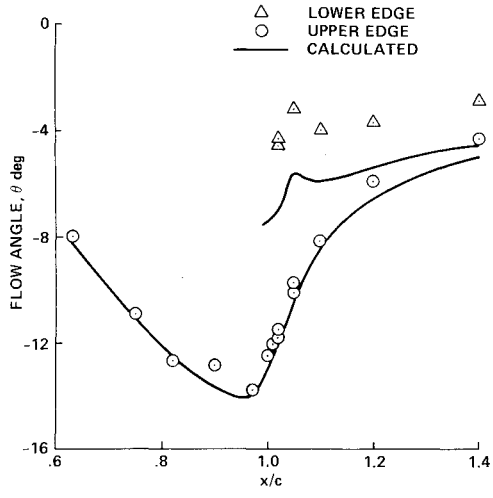

Fig. 8 Flow angles at edge of viscous layer in the vicinity of the trailing edge at cruise condition.

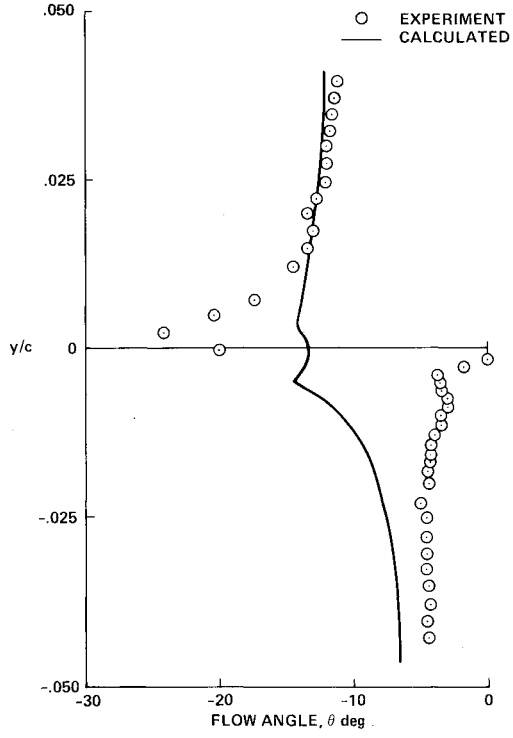

Fig. 9 Comparison of measured and predicted flow angles at $x/c=1.02$ for cruise condition.

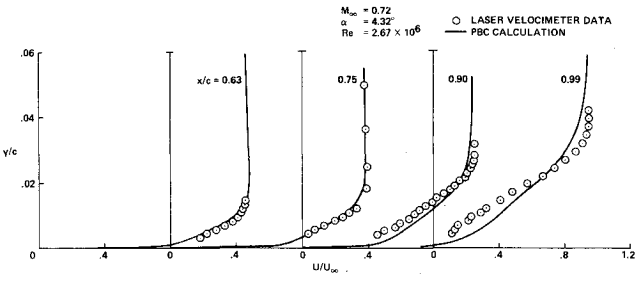

Fig. 10 Velocity profiles in the boundary layer at cruise condition.

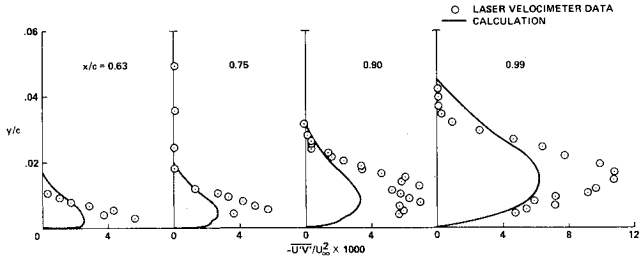

Fig. 11 Turbulent shear stresses in the boundary layer at cruise condition.

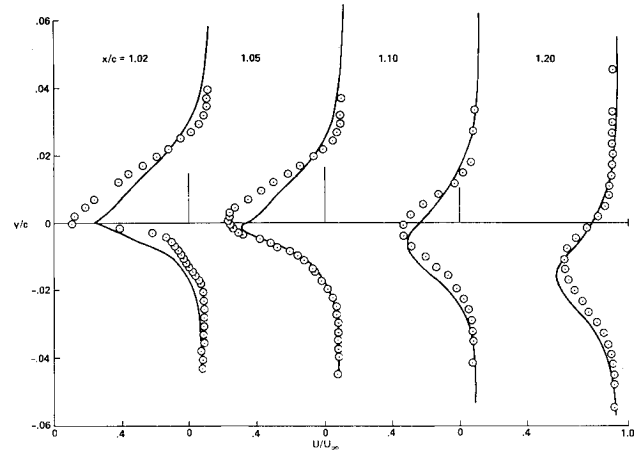

Fig. 12 Velocity profiles in the wake for cruise condition.

calculated profile has a very thin reversed-flow region above which high gradients exist.

In the authors' experience, it is seemingly characteristic of algebraic turbulence models, such as the one used herein, to overpredict the gradients in the near-wall region as separation is approached. This characteristic has been observed in transonic calculations for a conventional airfoil.[15] Horstman[21] obtained similar results in the trailing-edge region using a Cebeci-Smith model. In that same study, improved results were obtained with a two-equation turbulence model.

Turbulent shear-stress profiles for the upper boundary layer are presented in Fig. 11 at the same chordwise stations as the velocity profiles of Fig. 10. Two things are immediately apparent from these comparisons of the experimental velocity correlation with predicted values: 1) the predicted turbulent shear stresses extend to a larger distance above the airfoil as a consequence of the greater predicted boundary-layer thickness, and 2) maximum values of the predicted stresses are far less than those measured. Part of the reason for the higher measured values is that they are not in a surface-aligned coordinate system; however, that is insufficient to explain the large discrepancy. Although not shown, predictions in front of the shock agree well with experiment. The obvious conclusion, then, is that the turbulence model is inadequate in the high adverse-pressure-gradient region from the shock to the trailing edge.

Characteristics exhibited by the boundary layer toward the trailing edge of the airfoil are carried into the near wake. This is shown in Fig. 12 for the velocity profiles. Minimum velocities are greater than those measured, velocity gradients in the outer region of the wake are too low, and the wake is too thick. As the wake evolves to the far wake, the velocity profiles are in better agreement with the data, but the predicted wake position is lower than observed experimentally.

Examination of Fig. 12 reveals why the predicted flow angles in the near wake at $x/c = 1.02$, shown in Fig. 9, were at such large variance with experimental results. In the inner region of the wake, predicted horizontal velocities are greater than the data above the minimum velocity. This results in flow angles of smaller magnitude than the experiment, as is indeed demonstrated in Fig. 9. Below the minimum velocity line, predicted horizontal velocities are less than the data, thus the magnitude of the flow angles there exceeds the data. The large jump in flow angle at the minimum velocity was not seen since the predicted minimum velocity was much greater than the experiment. Also, it can be pointed out that the inadequacy of the turbulence model in high adverse-pressure-gradient regions is the reason for the poor velocity predictions at $x/c = 1.02$.

Concluding Remarks

Extensive comparisons have been made between Navier-Stokes calculations of supercritical airfoil flows and wind tunnel data. It has been demonstrated that wall-interference effects are important and must be accounted for in the calculations in order to make valid comparisons. The use of measured rail pressures above and below the airfoil as boundary data in the calculations has been shown to be an effective means of simulating the actual wind tunnel flow about an airfoil. Correction methods can be adequate to yield an equivalent free-air solution if surface pressures are the only concern.

Since measured pressures were used as boundary data and a fine calculational mesh was employed, the authors are confident that the differences between measurements and predictions are mainly attributable to the turbulence closure model. The Baldwin-Lomax turbulence model has been demonstrated to be inadequate in adverse pressure gradients, leading to reduced normal gradients of velocity in the outer region of the boundary layer and an overprediction of boundary-layer thickness. The algebraic turbulence model also failed to adequately describe the near-wall region in separating flows. Calculations and experiment indicate significant pressure differences can exist across the wake just behind the trailing edge of a supercritical section. Flow angles at the edges of the wake are fairly well predicted, but are in poor agreement through the near wake. This is a consequence of poor near-wake horizontal velocity predictions arising from inadequacies in near-wall turbulence modeling for flow separation.

References

[1]Spaid, F. W. and Bachalo, W. D., "Experiments on the Flow About a Supercritical Airfoil, Including Holographic Interferometry," *Journal of Aircraft*, Vol. 18, April 1981, pp. 287-294.

[2]Johnson, D. A. and Spaid, F. W., "Supercritical Airfoil Boundary-Layer and Near-Wake Measurements," *Journal of Aircraft*, Vol. 20, April 1983, pp. 298-305.

[3]Melnik, R. E., Chow, R., and Mead, H. R., "Theory of Viscous Transonic Flow Over Airfoils at High Reynolds Number," AIAA Paper 77-680, 1977.

[4]Melnik, R. E., "Turbulent Interactions on Airfoils at Transonic Speeds—Recent Developments," *AGARD Conference on Computation of Viscous-Inviscid Interactions*, AGARD CP-291, Paper 10, 1980.

[5]Kline, S. J., Cantwell, B. J., and Lilley, G. M., eds., *Proceedings, 1980-81 AFOSR-HTTM-Stanford Conference on Complex Turbulent Flows*, Vol. II, 1982, pp. 770-802.

[6]Kemp, W. B. Jr., "Toward the Correctable-Interference Transonic Wind Tunnel," *Proceedings of AIAA 9th Aerodynamic Testing Conference*, 1976, pp. 31-38.

[7]Kemp, W. B. Jr., "Transonic Assessment of Two-Dimensional Wind Tunnel Wall Interference Using Measured Wall Pressures," NASA CP-2045, 1979, pp. 473-486.

[8]Kemp, W. B. Jr., "TWINTAN: A Program for Transonic Wall Interference Assessment in Two-Dimensional Wind Tunnels," NASA TM 81819, May 1980.

[9]Murman, E. M., "A Correction Method for Transonic Wind Tunnel Wall Interference," AIAA Paper 79-1533, 1979.

[10]Steger, J. L., "Implicit Finite-Difference Simulation of Flow About Arbitrary Two-Dimensional Geometries," *AIAA Journal*, Vol. 16, July 1978, pp. 679-686.

[11]Beam, R. and Warming, R. F., "An Implicit Finite-Difference Algorithm for Hyperbolic Systems in Conservation-Law Form," *Journal of Computational Physics*, Vol. 22, Sept. 1976, pp. 87-110.

[12]Beam, R. and Warming, R. F., "An Implicit Factored Scheme for the Compressible Navier-Stokes Equations," *AIAA Journal*, Vol. 16, April 1978, pp. 393-402.

[13]Baldwin, B. S. and Lomax, H., "Thin Layer Approximation and Algebraic Model for Separated Turbulent Flows," AIAA Paper 78-257, 1978.

[14]Cebeci, T., "Calculation of Compressible Turbulent Boundary-Layers with Heat and Mass Transfer," *AIAA Journal*, Vol. 9, June 1971, pp. 1091-1097.

[15]King, L. S. and Johnson, D. A., "Calculations of Transonic Flow About an Airfoil in a Wind Tunnel," AIAA Paper 80-1366, 1980.

[16]Thompson, J. F., Thames, F. C., and Mastin, C. M., "Automatic Numerical Generation of Body-Fitted Curvilinear Coordinate System for Field Containing any Number of Arbitrary Two-Dimensional Bodies," *Journal of Computational Physics*, Vol. 15, 1974, pp. 299-319.

[17]Steger, J. L. and Sorenson, R. L., "Automatic Mesh-Point Clustering Near a Boundary in Grid Generation with Elliptic Partial Differential Equations," *Journal of Computational Physics*, Vol. 33, 1979, pp. 405-410.

[18]Bachalo, W. D., "An Experimental Investigation of Supercritical and Circulation Control Airfoils at Transonic Speeds Using Holographic Interferometry," AIAA Paper 83-1793, 1983.

[19]Murman, E. M., Bailey, F. R., and Johnson, M. J., "TSFOIL—A Computer Code for Two-Dimensional Transonic Calculations Including Wind Tunnel Wall Effects and Wave Drag Evaluation," NASA SP-374, 1975, pp. 749-768.

[20]Arieli, R. and Murphy, J. D., "Pseudo-Direct Solutions to the Boundary Layer Equations for Separated Flow," *AIAA Journal*, Vol. 18, Aug. 1980, pp. 883-891.

[21]Horstman, C. C., "Prediction of Separated Asymmetric Trailing Edge Flows at Transonic Mach Numbers," AIAA Paper 82-1021, 1982.